Inorganic Chemistry
Cite This: Inorg. Chem. 2019, 58, 1806−1814
Article
pubs.acs.org/IC

Strong Fluorescent Lanthanide Salen Complexes: Photophysical Properties, Excited-State Dynamics, and Bioimaging

Yuhang Yao,[†] Hao-Yan Yin,[†] Yingying Ning,[†] Jian Wang,[‡] Yin-Shan Meng,[†] Xinyue Huang,[§] Wenkai Zhang,[§] Lei Kang,[∥] and Jun-Long Zhang*[,†]

[†]Beijing National Laboratory for Molecular Sciences, State Key Laboratory of Rare Earth Materials Chemistry and Applications, College of Chemistry and Molecular Engineering, Peking University, Beijing 100871, People's Republic of China

[‡]Laboratory of Theoretical and Computational Chemistry, Institute of Theoretical Chemistry, Jilin University, Changchun 130023, People's Republic of China

[§]Center for Advanced Quantum Studies, Department of Physics and Applied Optics Beijing Area Major Laboratory, Beijing Normal University, Beijing 100875, People's Republic of China

[∥]Department of Nuclear Medicine, Peking University First Hospital, Beijing 100034, People's Republic of China

Supporting Information

ABSTRACT: The synthesis, excited-state dynamics, and biological application of luminescent lanthanide salen complexes (Ln = Lu, Gd, Eu, Yb, salen = *N*,*N*′-bis(salicylidene)ethylenediamine-based ligands) with sandwich structures are described. Among them, Lu(III) complexes show unusually strong ligand-centered fluorescence with quantum yields up to 62%, although the metal center is close to a chromophore ligand. The excited-state dynamic studies including ultrafast spectroscopy for Ln-salen complexes revealed that their excited states are solely dependent on the salen ligands and the ISC rates are slow (10^8−10^9 s^{-1}). Importantly, time-dependent density functional theory calculations attribute the low energy transfer efficiency to the weak spin−orbital coupling (SOC) between the singlet and triplet excited states. More importantly, Lu-salen has been applied as a molecular platform to construct fluorescence probes with organelle specificity in living cell imaging, which demonstrates the advantages of the sandwich structures as being capable of preventing intramolecular metal−ligand interactions and behaviors different from those of the previously reported Zn-salens. Most importantly, the preliminary study for in vivo imaging using a mouse model demonstrated the potential application of Ln coordination complexes in therapeutic and diagnostic bioimaging beyond living cells or in vitro.

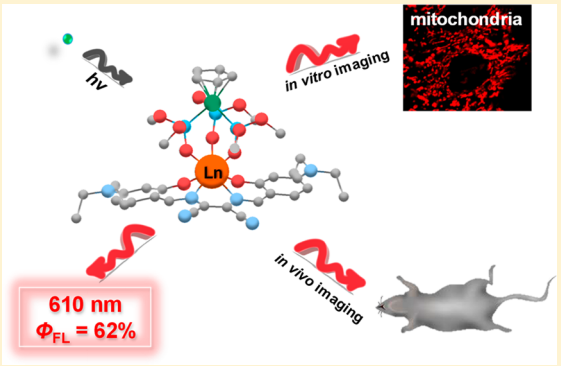

INTRODUCTION

Coordinating late transition metals to organic chromophore ligands is well-known to promote spin−orbit coupling (SOC) arising from heavy-metal effects and accelerate intersystem crossing (ISC) from singlet (S) to triplet (T) states. This thus leads to phosphorescence accompanied by the quenched fluorescence.[1] This view, however, is challenged by the increasing number of d-block transition-metal complexes featuring strong fluorescence under aerated conditions.[2] It has become clear that incorporation of a heavy metal does not guarantee enhanced SOC or efficient ISC, where the metal contribution to the excited states should be considered.[2,3] In contrast to d-block complexes, most fluorescent f-block lanthanide complexes previously reported have been dependent on f−f transitions rather than ligand-centered emission due to their large atomic numbers.[4] They have been long assumed to have efficient ISC during the sensitization process, in which energy transfer from the triplet state of the chromophore ligand to the excited state of Ln occurs intramolecularly.[5] Therefore, reference to new insights gained from d-block complexes, in revisiting the ISC process, is of fundamental importance and is highly desirable for the design of luminescent Ln coordination compounds.[2,3b,f,h]

N,*N*′-bis(salicylidene)ethylenediamine-based ligands, often abbreviated as "salen", are a class of extensively studied ligands prepared through the condensation of 2 equiv of salicylaldehyde and 1 equiv of ethylenediamine.[6] As tetradentate ligands, salens are able to stabilize lanthanide ions and provide flexible coordination spheres as well as light-harvesting antennas to sensitize lanthanide luminescence arising from the forbidden f−f transition.[7] Over the past decades, much attention has been focused on the construction of Ln-salen complexes with variable novel structures and magnetic and optical properties.[8] Several examples of lanthanide complexes exhibited ligand-centered emission;[9] however, their luminescence quantum

Received: August 22, 2018
Published: December 21, 2018

DOI: 10.1021/acs.inorgchem.8b02376
Inorg. Chem. 2019, 58, 1806−1814

efficiencies were still very low.[7,8] In addition, Wong and co-workers have reported a series of 3d−4f heterobimetallic lanthanide salen complexes, which also display fluorescence.[9]

As part of our longstanding research to explore the strongly luminescent Ln complexes, we herein chose 3-bis[(4-dialkylamino-2-hydroxybenzylidene)amino]but-2-enedinitrile ligands, containing both an electron-withdrawing cyano group and an electron-donating dialkylamino substituent, to sensitize Ln emission. We envisioned that, analogously to Ln porphyrinates,[10] such sandwich coordination structures render effective sensitization of Ln for the close distance between the Ln center and salen chromophore ligands, facilitating energy transfer from the ligand to the Ln centers. In this work, we report the synthesis of Ln-salen complexes (Lu, Eu, Yb, and Gd) and, beyond our expectations, found strong ligand-centered fluorescence with quantum yields up to 62%. To understand the nature behind Ln coordination, a combination of excited-state dynamic studies as well as theoretical calculations suggested that the slow ISC process arising from ineffective SOC could be attributed to the strong ligand-centered fluorescence. More importantly, Lu-salens have been demonstrated as molecular platforms to construct fluorescent bioprobes for living cell imaging, featuring a robust sandwich structure with a Kläui ligand and minimizing intermolecular metal−ligand interactions. Most importantly, Lu-salen was successfully applied to in vivo imaging using a mouse model, revealing the potential role of lanthanide coordination complexes in bioimaging that is not only limited to living cells or in vitro studies.

RESULTS AND DISCUSSION

Synthesis and Characterization. Ln-salen complexes were synthesized according to the previously reported methods as shown in Scheme 1a.[11] Treatment of free salen ligands (**L1** or **L2**), $Ln(acac)_3$ (acac = acetylacetone, Ln = Lu, Gd, Eu, Yb), and the Kläui tripodal ligand $[Na(\eta^5\text{-}C_5H_5)Co\{P(=O)(OMe)_2\}_3]$ (NaL_{OMe}) with the deprotonation of the free ligands by using triethylamine in a mixed solution of methanol and acetonitrile (1/1) afforded **LnL1** or **LnL2** complexes in 50−60% yields. To achieve biocompatibility and water solubility,[12] we introduced the phosphonium "onium" group, known to specifically target mitochondria, and prepared **LuL3** by transmetalation with **ZnL3**.[12,13] These Ln compounds were characterized by ^1H and ^{31}P NMR spectroscopy, electrospray ionization mass spectrometry (ESI-MS) and IR spectroscopy (Figures S1−S26 in the Supporting Information). ^1H NMR spectra of **LuL1**−**LuL3** showed the proton signals of imine and cyclopentadienyl groups of the Kläui tripodal ligand in the ranges of 8.08−8.19 and 4.91−4.93 ppm, respectively (Figures S3, S6, and S7). Due to unpaired f electrons of Ln atoms such as Eu and Yb, **EuL1** and **YbL1** showed proton signals but with paramagnetic shifts in comparison to Lu complexes. For example, the proton signals of imine and cyclopentadienyl groups in the Kläui tripodal ligand of **EuL1** appear in 4.02 and 2.89 ppm, respectively (Figure S4), while **YbL1** exhibits the protons of the imine moiety and Kläui ligand at 11.69 and 0.49 ppm (Figure S5). In ^{31}P NMR spectra, the P signals of the Kläui tripodal ligand for **LuL1**−**LuL3** appear at 117.7−118.6 ppm and the P signals of the phosphonium group of **LuL3** appear at 23.8 ppm (Figures S8, S11, and S12). The P signals of the Kläui tripodal ligand in **EuL1** and **YbL1** appear at 13.5 and 99.7 ppm, respectively (Figures S9 and S10).

Scheme 1. (a) Synthesis Routes of LnL1 (Ln = Lu, Gd, Eu, Yb), LnL2 (Ln = Lu, Gd), and LuL3 and Single-Crystal Structures of (b) LuL1 and LuL2[a]

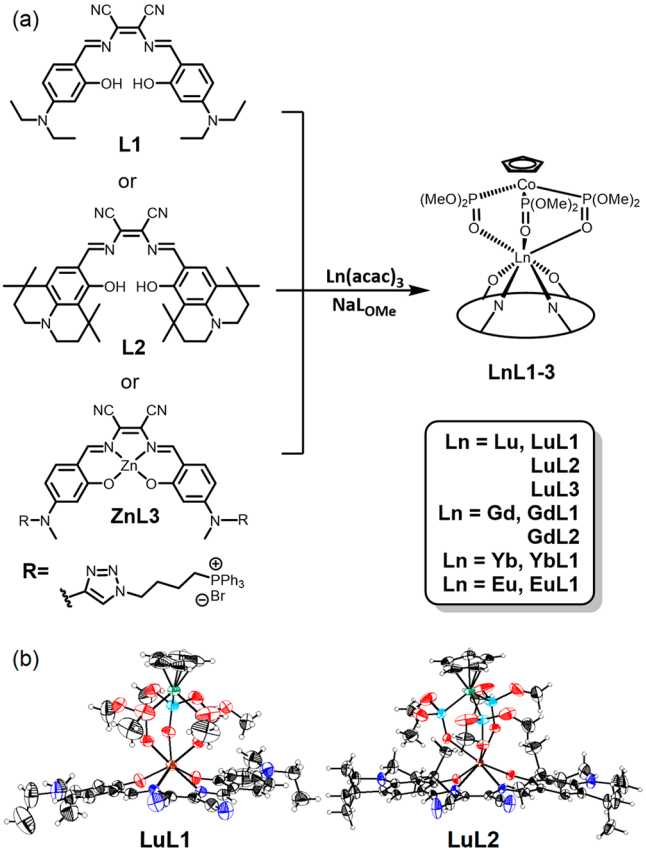

[a]The thermal ellipsoids are scaled to the 50% probability level, and solvent molecules are omitted for clarity.

X-ray Crystallography. Several single crystals of **LnL1** and **LnL2** suitable for X-ray diffraction were obtained by evaporation of the solvent from a mixed solution of CH_2Cl_2 and petroleum ether (CCDC 1568442, 1568443, 1568448, 1568449, 1568452 and 1836024 in Tables S1 and S2). **LuL1**, **GdL1**, and **YbL1** crystallize in a triclinic space group, and **EuL1**, **LuL2**, and **GdL2** crystallize in a monoclinic space group (Tables S1 and S2). As shown in Scheme 1b and Figures S27−S30, these Ln-salen complexes display a seven-coordination environment around the lanthanide center, which is sandwiched between the salen and the Kläui tripodal ligands. The salen ligands of **LnL1** and **LnL2** series are planar, which is different from the case for polynuclear lanthanide salen complexes[7,9,14] but similar to the the case for previously reported zinc,[12] platinum,[15] and palladium[15b] salen complexes.

To better illustrate the metal effect, we compared the structural information of **LnL1** with the same salen ligands. As shown in Table 1 and Table S3, the average lengths of Ln−O and Ln−N bonds are in the ranges 2.220−2.306 and 2.419−2.524, Å respectively, in the order of Ln(III) ion radius (**EuL1** > **GdL1** > **YbL1** > **LuL1**). The distance between the metal center and the N_2O_2 mean plane in **GdL1** (1.010 Å) is shorter than those of **YbL1** (1.047 Å), **LuL1** (1.046 Å), and **EuL1** (1.070 Å). In comparison with previously reported Ln porphyrinate analogues (~1.308 Å for Gd and 1.209−1.215 Å for Yb),[10a,11b,16] **YbL1** and **GdL1** showed slightly smaller displacements of the metal center out of the N_2O_2 mean plane

DOI: 10.1021/acs.inorgchem.8b02376
Inorg. Chem. 2019, 58, 1806−1814

Table 1. Summary of the Ln−O and Ln−N Bond Distances, Ln to Plane Center Distances, and Dihedral Angles between N_2O_2 and O_3 planes

	LuL1	GdL1	EuL1	YbL1	LuL2
		Distances (Å)			
av Ln−O	2.220	2.298	2.306	2.226	2.220
av Ln−N	2.434	2.522	2.524	2.445	2.419
$Ln-N_2O_2$	1.046	1.010	1.070	1.047	1.111
$Ln-O_3$	1.532	1.620	1.605	1.533	1.533
		Dihedral Angles (deg)			
$\angle N_2O_2-O_3$	179	175	170	179	176

(1.047 and 1.010 Å, respectively) in the presence of the Kläui ligand, indicating that the Ln ion is located close enough to the chromophore ligands.

The ligand effect was also investigated by comparison of the structures of **LuL1** and **LuL2**. The average Lu−O (2.220 Å for **LuL1** and **LuL2**) and Lu−N (2.434 Å for **LuL1** and 2.419 Å for **LuL2**) distances are almost the same. The Lu(III) ion is located 1.046 Å above the N_2O_2 mean plane and 1.532 Å under the O_3 plane for **LuL1**, similar to the distances of **LuL2** (1.111 Å above the N_2O_2 mean plane and 1.533 Å under the O_3 plane). The N_2O_2 and O_3 planes are almost planar (179 and 176° for **LuL1** and **LuL2**, respectively). These results suggested that substitution at the salicylaldehyde moiety have a slight effect on Ln coordination.

Photophysical Properties. Absorptions of **LnL1**−**LnL3** were recorded at 298 K in CH_2Cl_2 (Figure 1 and Figures S31 and S32), and the photophysical data are given in Table 2. For example, **LnL1** shows a sharp band with a maximum centered at 377−381 nm with a shoulder at ca. 435 nm and an intense absorption maximum at 573 nm, similar to those of free base ligand and Zn-salen.[17] They are different from their Pt and Pd counterparts, which display absorption maxima at 560 and 596 nm arising from metal−ligand charge transfer (MLCT).[15b] Ln coordination resulted in a small bathochromic shift (~3 nm) of absorption with respect to the free ligand. Replacing Lu with Gd, Eu, and Yb has a very slight influence on the absorption, indicating that the nature of the metal ions plays only a minor role in the electronic structures of the frontier molecular orbitals. The intense absorption manifold of the **LnL1** maximum at 573 nm manifests a full width at half maximun (fwhm) of ~1250 cm^{-1} and less discernible vibrational structures, suggesting that the **LuL1** chromophores have an intraligand transition of CT character. This is supported by theoretical computations in this context. **LuL2** and **GdL2** exhibit a similarly strong absorption centered at 392 nm with a shoulder at ca. 455 nm and an intense band maximum at ca. 600 nm in MeOH (Figure S31 and Table 2), and **LuL3** displays a hypsochromically shifted absorption in comparison with **LuL1** (Figure S32 and Table 2).

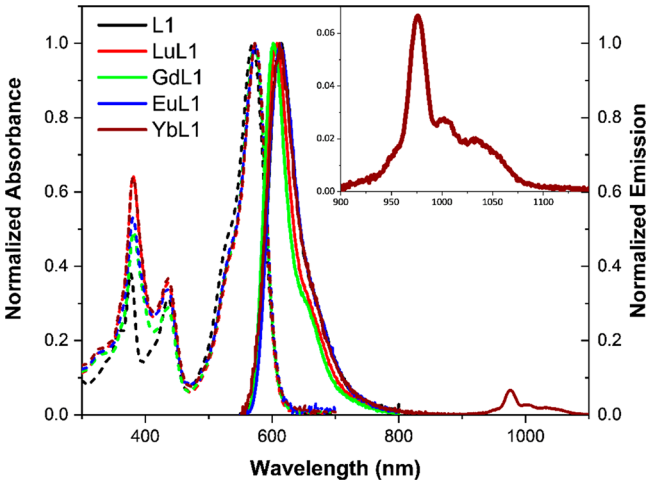

Figure 1. Normalized electronic absorption (dashed line) and emission (solid line) spectra of the **LnL1** series in CH_2Cl_2 (inset: near-IR luminescence of **YbL1**).

Upon excitation at 573 nm, Ln complexes exhibit a ligand-centered fluorescence maximum at ca. 610 nm (Figure 1 and Figures S31−S62), insensitive to air or oxygen (Figures S63−S69). Even at 77 K, no phosphorescence was observed (Figures S70−S78). Nanosecond time-resolved emission (ns-TRE) spectra of **LnL1** complexes (Ln = Lu, Gd, Yb) showed emission decay with a single component, as presented in Figures S79−S83. Thus, the emission is not from the low-lying triplet excited state of the ligand or MLCT, different from the case for previously reported Pt[15,18] and Pd[15b,19] salen complexes. As expected, **YbL1** exhibits ligand-centered fluorescence with the appearance of NIR emission of the Yb^{3+} ion at 900−1100 nm with a lifetime of 16 μs, arising from a $^2F_{5/2} \rightarrow {}^2F_{7/2}$ transition. This suggests that energy transfer from salen ligand to the Yb^{3+} center is similar to those of the previously reported polynuclear Yb(III) salen complexes.[7b,20] We also recorded the concentration-dependent emission in CH_2Cl_2 and water. As shown in Figure S34, the emission intensity of **LuL1** increases linearly with concentration up to 0.4 mM in CH_2Cl_2. However, the fluorescent intensity of **LuL3** increases linearly with concentration from 3.33×10^{-3} to 3.33×10^{-2} mM and then decreases when the concentration larger than 3.33×10^{-2} mM due to the limited solubility in water.

Transient Absorption Spectroscopy. Insights into the nature of the photodynamic processes, exemplified by **LnL1**, were obtained using nanosecond (ns-TA) and femtosecond (fs-TA) transient absorption spectroscopy. Figure 2a shows the intense positive absorptions for **LuL1** from $T_1 \rightarrow T_n$ transitions centered at 410, 480, and 625 nm, accompanied by the ground-state bleaching (GSB) maxima at 380, 450, and 575 nm. A similar ns-TA spectrum was observed for **GdL1** (Figure 2b). The triplet-state decay lifetimes of **LuL1** and **GdL1** were determined to be 80.0 and 16.0 μs in degassed CH_2Cl_2 and decreased to 0.81 and 0.50 μs under air-saturated conditions (Figure S84), respectively. The shorter lifetime of **GdL1** might be due to unpaired f electrons of Gd^{3+} in comparison to those of **LuL1**. **YbL1** exhibited a smaller ΔOD value (Figure 2c) in comparison to **LuL1** and **GdL1**, which is ascribed to energy transfer from the triplet state of the ligand to the excited state of Yb^{3+}.[11b] Thus, ns-TA spectroscopic studies confirmed the population of the triplet excited state of **LnL1** upon photoexcitation similar to that of **L1** (Figure S85). Figure 2d−f shows fs-TA spectra for **LuL1**, **GdL1**, and ligand **L1** with a time window of approximate 3.50 ns. We observed a decay of the GSB band maximum at 575 nm and a simultaneous rise in the excited-state absorption (ESA) band centered at ca. 680 nm. These compounds display triple-exponential decay lifetimes (1.00−3.50 ps, 78.0−128.0 ps, and 1.00−2.51 ns) as monitored at 672−700 nm, indicating at least three relaxation processes (Figure 2d−f). The two fast-decay processes were assumed to be solvation (<10 ps) and structural relaxation dynamics (~100 ps). The nanosecond

DOI: 10.1021/acs.inorgchem.8b02376
Inorg. Chem. 2019, 58, 1806−1814

Table 2. Absorption and Luminescence Data of LnL1 in CH_2Cl_2 at Room Temperature

compound	λ_{max}/nm (log ε)	λ_{em}/nm	Φ/%[a]	τ/ns[b]
LuL1	381 (4.85), 435 (4.61), 573 (5.05)	608	62	2.99
GdL1	381 (4.72), 435 (4.23), 573 (5.03)	602	19	0.87 (23%), 2.29 (77%)
EuL1	381 (5.10), 434 (4.95), 573 (5.25)	613	11	2.50
YbL1	381 (4.89), 435 (4.65), 573 (5.09)	612, 976, 1002, 1033	6.8[c]	0.73 (63%), 3.40 (37%), 16 μs[d]
LuL3	376 (4.53), 426 (4.29), 565 (4.62)	601	53	2.94
LuL2	392 (4.90), 455 (4.55), 600 (4.79)	642	31	2.53
GdL2	392 (4.78), 456 (4.57), 597 (4.99)	652	45	0.49 (10%), 2.40 (90%)

[a]Referenced to the ligand-centered fluorescence in CH_2Cl_2 solution at room temperature. Absolute quantum yields (Φ_s) were determined on an Edinburgh Analytical Instrument FLS-980 equipped with an integrating sphere. [b]Determined in CH_2Cl_2 solution at room temperature. Gd and Yb complexes show fluorescence with two-component lifetimes, while other complexes show fluorescence with single-component lifetimes. [c]For **YbL1**, the emission maximum at 612 nm refers to ligand-centered fluorescence and the NIR emission is from a f−f transition of Yb^{3+}, which is too weak for a determination of Φ. [d]Kinetic decay at 1002 nm.

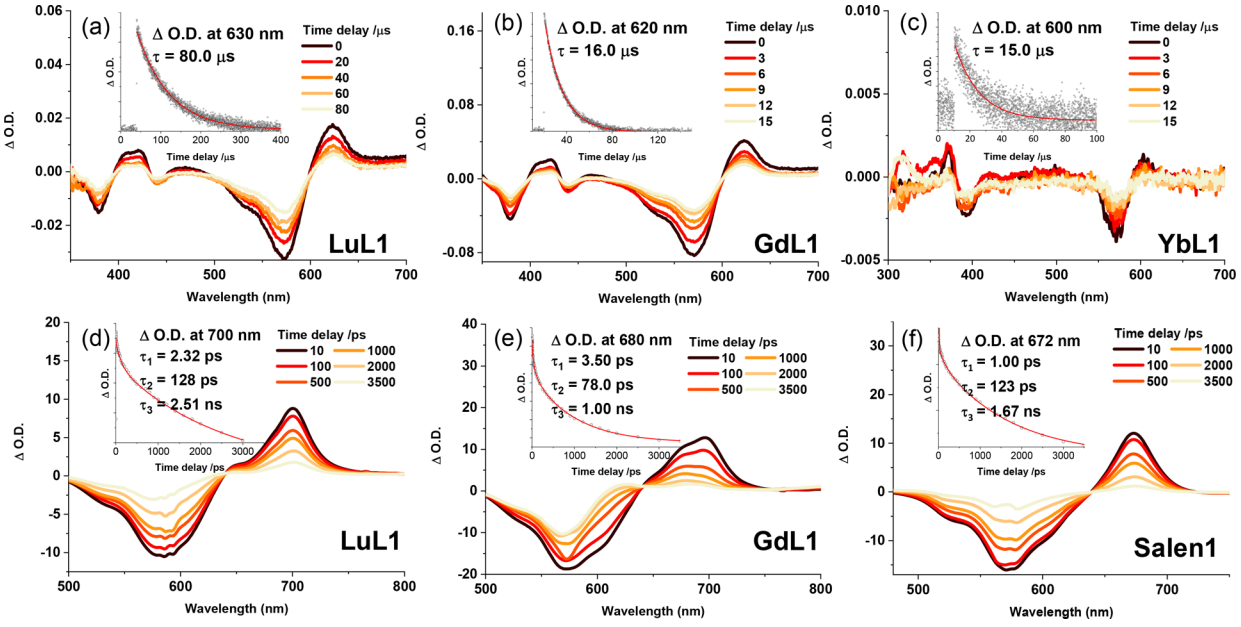

Figure 2. Nanosecond transient absorption (ns-TA) difference spectra of (a) **LuL1**, (b) **GdL1**, and (c) **YbL1** recorded at selected decay times in degassed CH_2Cl_2 at 298 K. Femtosecond transient absorption (fs-TA) difference spectra of (d) **LuL1**, (e) **GdL1**, and (f) **L1** recorded at selected decay times in CH_2Cl_2 at 298 K. Insets show the ESA kinetic decay traces at the specified wavelengths and lifetimes, which were fitted to a single-exponential decay for ns-TA and a triple-exponential decay for fs-TA.

component is assigned to the intrinsic S_1 state lifetime, which is comparable to the fluorescence lifetimes. In this work, we could not observe phosphorescence; this might be due to the triplet states not being emissive or the ISC process is slow for inefficient SOC, despite the Ln center being close enough (~1 Å) to chromophore ligands. With reference to Pt or Pd salen counterparts even with the same ligand,[15b] which display strong phosphorescence arising from the triplet intraligand transition or ^{3}MLCT,[21] we tentatively excluded the possibility that the triplet states are not emissive. Thus, we ascribed strong fluorescence to slow ISC due to inefficient SOC.

To estimate ISC efficiency, we assumed that the major nonradiative decay of the S_1 state is ISC: i.e. $k_{nr} \approx k_{ISC}$. On the basis of the fluorescence quantum yields (Φ_F) and the lifetimes (τ_f) for **LnL1**, an upper bound approximation of k_{ISC} values and quantum yields (Φ_{ISC}) of ISC could be calculated, as shown in Table 3. **LuL1** shows the highest radiative decay rate ($k_F = 2.07 \times 10^8$ s^{-1}) from the S_1 to S_0 state among the four complexes. The lower ISC efficiency (38%) for **LuL1** was obtained on the basis of the slow ISC rate (1.28×10^8 s^{-1}) in comparison to those of **GdL1**, **GdL1**, and **YbL1**. Thus, it is not surprising that **LuL1** could emit strong fluorescence but not phosphorescence due to the low ISC efficiency. **GdL1** and **EuL1** exhibited a faster ISC process (10^8−10^9 s^{-1}) and displayed a higher ISC quantum yield (81% for **GdL1** and 89% for **EuL1**) in comparison to **LuL1**. This is probably due to the unpaired 4f electrons accelerating spin−orbital coupling.[22]

Table 3. Excited-State Relaxation Dynamic Data, Fluorescence Quantum Yields, and ISC Efficiencies for the LnL1 Series Determined in CH_2Cl_2

		relaxation rate from S_1/s^{-1}			
compd	τ_{s1}/ns	$k_F(S_1 \rightarrow S_0)$[a]	$k_{ISC}(S_1 \rightarrow T_1)$[a]	Φ_F/%	Φ_{ISC}/%
LuL1	2.99	2.07×10^8	1.28×10^8	62	38
GdL1	2.29	8.30×10^7	3.54×10^8	19	81
EuL1	2.50	4.40×10^7	3.56×10^8	11	89
YbL1	0.73	9.32×10^7	1.28×10^9	6.8	93

[a]k_F denotes the intrinsic fluorescence rate constant, and k_{ISC} denotes the $S_1 \rightarrow T_1$ ISC rate constant. Excited-state relaxation rate constants were calculated on the basis of the following equations: $\tau_{s1} = 1/(k_F + k_{ISC})$, $\Phi_F = k_F \times \tau_{s1}$, $\Phi_{ISC} = k_{ISC} \times \tau_{s1}$, and $\Phi_F + \Phi_{ISC} = 1$.

DOI: 10.1021/acs.inorgchem.8b02376
Inorg. Chem. 2019, 58, 1806−1814

This could be supported by the comparison of decay rates between **GdL1** and **LuL1** in nanosecond transient absorption; the Lu complex is much slower (80 μs) than the Gd complex (16 μs). It is worth noting that the Yb complex displayed a faster ISC rate (1.28×10^9 s^{-1}) in comparison to the Lu, Gd, and Eu complexes (($(1.28-3.56) \times 10^8$ s^{-1}), indicating the possibility that the population of the triplet state of the ligand led to Yb emission. This could also be supported by the nanosecond transient absorption spectrum of the Yb complex, which showed a faster decay of the triplet state in comparison to that of the Lu complex and much lower ΔOD values in comparison to the Gd complex. A weak Yb emission at 900–1100 nm from a $^2F_{5/2} \rightarrow {}^2F_{7/2}$ transition was observed, and the lifetime (16 μs) was very short, which might be due to high vibrational C–H bond quenching or inefficient energy transfer. For **EuL1**, in which emissive states (for example, Eu $^5D_0$) are lying higher than the lowest triplet state of **L1**, we only observed ligand-centered fluorescence. In this work, for either Eu or Yb complexes, we could not exclude the mechanism of electron exchange between the excited singlet state of the ligand to metal center due to the lack of experimental evidence.

Theoretical Computation. To further understand the electronic structure of **LuL1**, DFT and TDDFT calculations at the level of B3LYP/6-311G(d)[23] (the Stuttgart relativistic pseudopotential and its accompanying basis set (ECP60MWB)[24] and the effective core potential (ECP) Lanl2DZ basis set[25] were used for Lu and Co atoms, respectively) in the Gaussian 09 package provided structural optimization and prediction of electronic absorption (Table S4 and Figures S86–S88). An interaction diagram of the fragment orbitals by charge decomposition analysis (CDA)[26] suggests that valence orbitals and low-lying virtual orbitals of **LuL1** are mainly localized in the salen ligand and axial ligand (Figure 3).

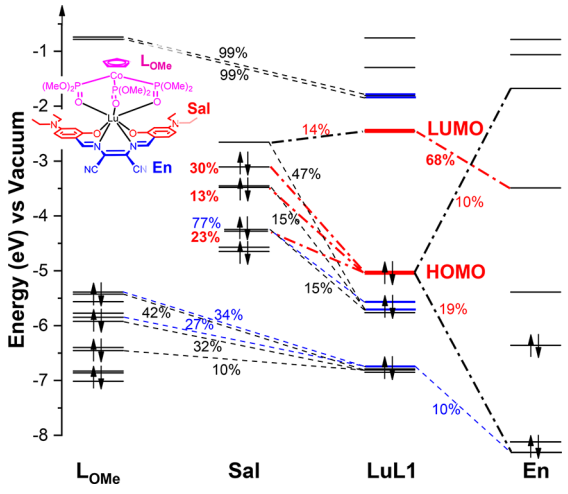

Figure 3. Interaction diagram of fragment orbitals determined by charge decomposition analysis (CDA) for **LuL1**.

This is in accordance with the absorption and emission spectra, which are less dependent on Ln ions. As shown in Figure 4a and Table S5, we calculated k_F and the rate of phosphorescence (k_P) for **LuL1** with the ADF 2016 program package using perturbative SOC-TDDFT.[27] The computed rate k_F from the S_1 to S_0 state is 2.74×10^8 s^{-1}, close to that found experimentally (2.07×10^8 s^{-1}). In addition, the calculated rate k_P from the T_1 to S_0 state is 15.6 s^{-1}. The energy separations $\Delta E(S_1-T_n)$ between S_1 and the T_1, T_2, and T_3 states are 5977,

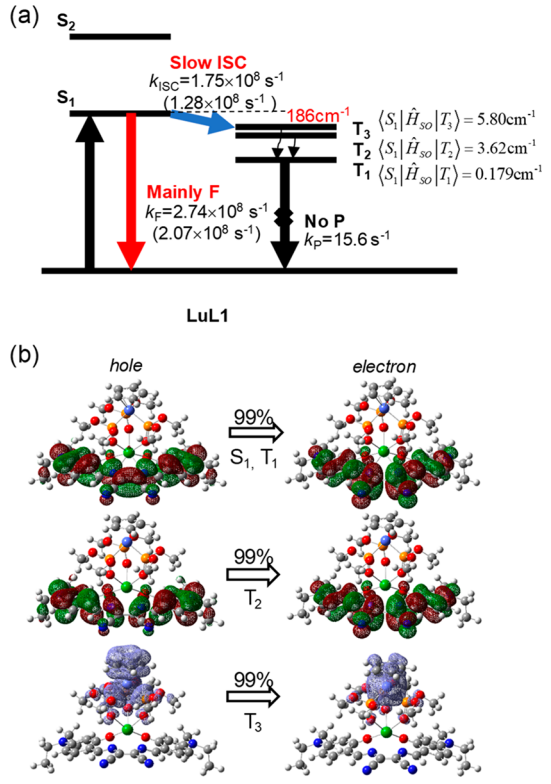

Figure 4. (a) Illustration of the low-lying singlet and triplet excited states of the **LuL1** complex and the calculated rate constants of different photophysical processes with experimental results in parentheses. (b) Pictorial representation of natural transition orbitals (h, hole; e, electron) of the S_1 and T_1–T_3 states for **LuL1**. The weight of the hole–electron contribution to the excitation is also included.

398, and 186 cm^{-1} (Table 4), respectively. In comparison with Pt and Pd salen complexes,[18] a small ΔE_{ST} value between the S_1 and T_3 states is a prerequisite for efficient ISC.

Table 4. Calculated Low-Lying Singlet and Triplet Excited States and the Nature of the Transitions at the Optimized Ground State Geometry of LuL1 in CH_2Cl_2

state	E (cm^{-1})	λ (nm)	major contribution[a]
T_1	12210	819.04	H → L (93%)
T_2	17789	562.16	H-1 → L (53%), H-2 → L (31%)
T_3	18001	555.52	H-6 → L+2 (21%), H-4 → L+1 (13%), H-12 → L+1 (10%), H-11 → L+2 (10%)
S_1	18187	549.86	H → L (99%)

[a]H = HOMO; L = LUMO.

The ISC rate constant (k_{ISC}) was theoretically estimated according to Fermi's golden rule and Marcus–Levich–Jortner theory (eq 1).[28]

$$k_{ISC} = \frac{2\pi}{\hbar} |\langle T_m|\hat{H}_{SO}|S_n\rangle|^2 \rho_{FC} \quad (1)$$

Two major factors, i.e. SOC matrix element (SOCME) and Franck–Condon weighted density of states (FCWD, ρ_{FC}), were used to evaluate k_{ISC}.[28] SOCMEs of **LuL1** (Figure 4b and Table S6) between S_1 and T_1 (0.179 cm^{-1}), T_2 (3.62 cm^{-1}), and T_3 (5.80 cm^{-1}) states are about 2 or 3 orders of magnitude smaller than those of the other heavy-metal salen complexes mentioned above, which should be the key point for such an

DOI: 10.1021/acs.inorgchem.8b02376
Inorg. Chem. 2019, 58, 1806–1814

inefficient ISC.[2a] We took the ISC process between S_1 and T_3 states as an example. The k_{ISC} value between S_1 and T_3 states was calculated to be 1.75×10^8 s^{-1} (Tables S7 and S8), in agreement with the experimental value of 1.28×10^8 s^{-1}. The theoretical results suggest that a small SOC and slow ISC process are the primary causes of the ligand-centered fluorescence for **LuL1**.

Bioimaging. The high extinction coefficients (ε) and quantum yields (Φ) contribute to the exceptional brightness of Lu-salens, which is of prime significance for their further applications as bioimaging probes. Lu-salens described in this work have sandwich structures which minimize intermolecular metal−ligand or metal−metal interactions, making them different from the previously reported luminescent metallo-salens.[6c,12,17,29]

We measured the absorption and emission of **LuL1** and **LuL3** in water. As shown in Figure S33, **LuL1** exhibits much broader and more red shifted bands in both absorption and emission spectra in comparison to **LuL3**. This suggests that **LuL1** tends to aggregate in water, while **LuL3** tends to form a monomer probably due to the water-soluble phosphonium ion. For the sandwich structures of Ln complexes in this work, we assumed that the driving force for the aggregation is their hydrophobicity rather than the intermolecular metal−ligand interaction observed in Zn-salen.[29d] The quantum yields of **LuL1** and **LuL3** were 0.21 and 0.55%, respectively, in water (Figures S61 and S62). Shorter lifetimes (0.31 ns for **LuL1** and 1.57 ns for **LuL3**; Figures S50 and S51) in comparison to those in CH_2Cl_2 were obtained, due to water possibly quenching the fluorescence.

As **LuL3** has better water solubility, we then assessed the stability and cytotoxicity of **LuL3** in aqueous media and living cells. It remained stable in water and phosphate buffer solution (PBS) for 12 h, with over 90% and 80% retention of the UV−vis absorbance (Figure S89), respectively. The stability was also retained after 1 h of white light irradiation (Figure S90). The cytotoxicity and photocytotoxicity of **LuL3** were measured by a CCK-8 tool kit, and HeLa cells possessed a high cell viability up to 90% under 8 μM **LuL3** incubation (Figure S91). Therefore, the high fluorescence, stability, and low cytotoxicity of Lu-salens make them potential live cell imaging agents.

The subcellular locations of **LuL1** and **LuL3** were investigated by laser scanning confocal microscopy (LSCM) in HeLa cells, and experimental details are given in the Supporting Information. As shown in Figure 5, **LuL1** was mainly located in lysosomes and was colocalized with the lysosome tracker LysoTracker Green DND-26 (the Pearson coefficient was 0.80). **LuL3** colocalized well with MitoTracker Green FM (the Pearson coefficient was 0.71), which is different from the case for the previously reported phosphonium ion modified Zn-salen. The phosphonium ion modified Zn-salen was located mainly in lysosomal and endosomal compartments due to the intermolecular metal−ligand interaction induced aggregation.[12,29d,30] **LuL3** was successfully directed into mitochondria by the targeting group triphenylphosphine ion, suggesting that the sandwich structure helps inhibit the aggregation process. Thus, Lu-salen is a decent fluorescent molecular platform with high brightness and possibility of further modifications for different organelles.

To demonstrate the potential application to in vivo bioimaging, we chose the nude mouse as an animal model using **LuL3** as the probe. A normal saline solution of **LuL3**

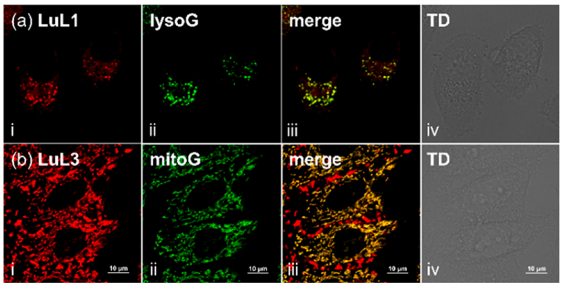

Figure 5. Colocalization assay of (a) **LuL1** with LysoTracker Green DND-26 and (b) **LuL3** with MitoTracker Green FM: (i) confocal fluorescence images of **LuL1** and **LuL3**; (ii) confocal fluorescence images of LysoTracker Green DND-26 and MitoTracker Green FM; (iii) merged confocal fluorescence images of (i) and (ii); (iv) differential interference contrast (DIC) images. Scale bar: 10 μm.

(100 uL, 2 mg/mL) was injected intravenously into the nude mouse via the tail vein and imaged with 570 nm excitation and 620 nm emission. Immediately after injection, the luminescence signal was weak (Figure S92). However, as shown in Figure 6a, after 30 min, strong in vivo fluorescence was

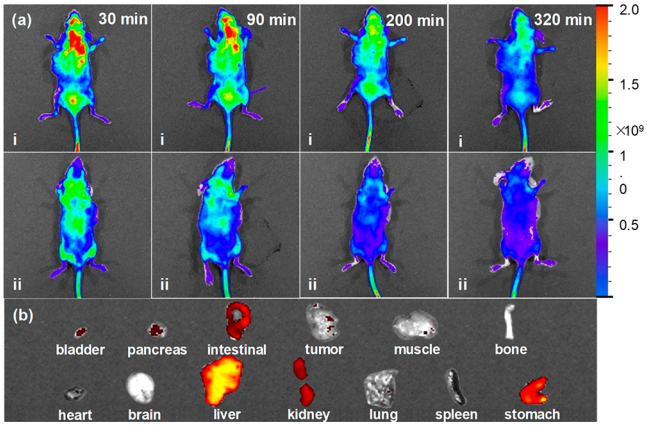

Figure 6. (a) In vivo fluorescence images (λ_{ex} 570 nm, λ_{em} 620 nm) of a 2-week-old nude mouse with a subcutaneous tumor after tail-vein injection of **LuL3** (100 μL, ~2 mg/mL) in the (i) supine and (ii) prone positions. (b) Ex vivo biodistribution studies of **LuL3** at 320 min after injection.

observed. The signals mainly accumulated in the liver and renal system, indicating that **LuL3** circuited quickly in the body with blood circulation. After 320 min, the in vivo fluorescence signals almost disappeared but very weak signals could be observed from the prone position. This suggested the short blood-circulation half-life of **LuL3**. Thereafter, the mouse was euthanized and dissected after 5 h postinjection to investigate the distribution of **LuL3** in major organs. As shown in Figure 6b, an ex vivo fluorescence study showed strong signals in the liver, kidney, intestine, and stomach, indicating that **LuL3** was mainly excreted through enterohepatic circulation and the digestive system. In bone, brain, tumor, heart, spleen, and lung, no luminescence signals were observed, suggesting that the cardiopulmonary system was not involved in the process and the complex was not able to cross the blood−brain barrier and accumulate in tumors without further modifications. However, the ex vivo experimental results highly matched the in vivo fluorescence results. This revealed that, although the excitation and emission wavelengths of the Lu complexes are in the

DOI: 10.1021/acs.inorgchem.8b02376
Inorg. Chem. 2019, 58, 1806−1814

visible region, their high quantum yields still render them potential in vivo fluorescence imaging agents.

CONCLUSIONS

The sandwich lanthanide salen complexes **LnL1**−**LuL3** were synthesized and characterized. The single-crystal structures suggested planar salen ligands for the **LnL1** and **LnL2** series, which are different from the case for previous polynuclear lanthanide salen complexes but similar to the case for the zinc and platinum salen complexes. Ligand-centered absorption and emission spectra revealed the minor effect of the lanthanides on the ground- and excited-state properties of the complexes. The combination of ultrafast transient spectroscopy and TDDFT calculations revealed that the nature of ligand-centered fluorescence resulted from weak spin−orbital coupling and thus inefficient intersystem crossing even with very little energy separation, which differed from the case for other heavy-metal salen complexes. Lutetium salen complexes were also applied to in vivo imaging using a mouse model, revealing the potential role of lanthanide coordination complexes in bioimaging that is not limited to living cells or in vitro studies and thus enriching the realm of metal bioprobes.

ASSOCIATED CONTENT

Supporting Information

The Supporting Information is available free of charge on the ACS Publications website at DOI: 10.1021/acs.inorgchem.8b02376.

Detailed synthesis, isolation, photophysical, and crystallographic data, ^{1}H and ^{31}P NMR, UV−vis absorption, IR, and HR-MS spectra, a detailed experimental section, and TD-DFT calculations (PDF)

Accession Codes

CCDC 1568442−1568443, 1568448−1568449, 1568452, and 1836024 contain the supplementary crystallographic data for this paper. These data can be obtained free of charge via www.ccdc.cam.ac.uk/data_request/cif, or by emailing data_request@ccdc.cam.ac.uk, or by contacting The Cambridge Crystallographic Data Centre, 12 Union Road, Cambridge CB2 1EZ, UK; fax: +44 1223 336033.

AUTHOR INFORMATION

Corresponding Author

*E-mail for J.-L.Z.: zhangjunlong@pku.edu.cn.

ORCID

Jun-Long Zhang: 0000-0002-5731-7354

Notes

The authors declare no competing financial interest.

ACKNOWLEDGMENTS

We acknowledge financial support from the National Key Basic Research Support Foundation of China (Grant 2015CB856301) and the National Scientific Foundation of China (Grants 21571007, 21271013, 21321001). This work was also supported by the High-performance Computing Platform of Peking University.

REFERENCES

(1) (a) Dearmond, M. K. Relaxation of excited states in transition-metal complexes. *Acc. Chem. Res.* **1974**, *7*, 309−315. (b) Fleischauer, P. D.; Fleischauer, P. Photoluminescence of transition metal coordination compounds. *Chem. Rev.* **1970**, *70*, 199−230. (c) Turro, N. J.; Ramamurthy, V.; Scaiano, J. C. *Principles of Molecular Photochemistry: an Introduction*; University Science Books: Sausalito, CA, 2009. (d) Zhao, Q.; Huang, C.; Li, F. Phosphorescent heavy-metal complexes for bioimaging. *Chem. Soc. Rev.* **2011**, *40*, 2508−2524. (e) Chergui, M. Ultrafast photophysics of transition metal complexes. *Acc. Chem. Res.* **2015**, *48*, 801−808. (f) Baryshnikov, G.; Minaev, B.; Agren, H. Theory and calculation of the phosphorescence phenomenon. *Chem. Rev.* **2017**, *117*, 6500−6537. (g) Penfold, T. J.; Gindensperger, E.; Daniel, C.; Marian, C. M. Spin-vibronic mechanism for intersystem crossing. *Chem. Rev.* **2018**, *118*, 6975−7025. (h) Zhang, K. Y.; Yu, Q.; Wei, H.; Liu, S.; Zhao, Q.; Huang, W. Long-lived emissive probes for time-resolved photoluminescence bioimaging and biosensing. *Chem. Rev.* **2018**, *118*, 1770−1839.

(2) (a) Tong, G. S.; Chow, P. K.; To, W. P.; Kwok, W. M.; Che, C. M. A theoretical investigation into the luminescent properties of d8-transition-metal complexes with tetradentate Schiff base ligands. *Chem. - Eur. J.* **2014**, *20*, 6433−6443. (b) Chan, K. T.; Tong, G. S. M.; To, W.-P.; Yang, C.; Du, L.; Phillips, D. L.; Che, C.-M. The interplay between fluorescence and phosphorescence with luminescent gold(I) and gold(III) complexes bearing heterocyclic arylacetylide ligands. *Chem. Sci.* **2017**, *8*, 2352−2364. (c) Bai, Y.; Rawson, J.; Roget, S. A.; Olivier, J.-H.; Lin, J.; Zhang, P.; Beratan, D. N.; Therien, M. J. Controlling the excited-state dynamics of low band gap, near-infrared absorbers via proquinoidal unit electronic structural modulation. *Chem. Sci.* **2017**, *8*, 5889−5901.

(3) (a) Heng, W. Y.; Hu, J.; Yip, J. H. K. Attaching gold and platinum to the rim of pyrene: a synthetic and spectroscopic study. *Organometallics* **2007**, *26*, 6760−6768. (b) Weissman, H.; Shirman, E.; Ben-Moshe, T.; Cohen, R.; Leitus, G.; Shimon, L. J.; Rybtchinski, B. Palladium complexes of perylene diimides: strong fluorescence despite direct attachment of late transition metals to organic dyes. *Inorg. Chem.* **2007**, *46*, 4790−4792. (c) Lentijo, S.; Miguel, J. A.; Espinet, P. Highly fluorescent platinum(II) organometallic complexes of perylene and perylene monoimide, with Pt σ-bonded directly to the perylene core. *Inorg. Chem.* **2010**, *49*, 9169−9177. (d) Steffen, A.; Tay, M. G.; Batsanov, A. S.; Howard, J. A.; Beeby, A.; Vuong, K. Q.; Sun, X. Z.; George, M. W.; Marder, T. B. 2,5-Bis(p-R-arylethynyl)-rhodacyclopentadienes show intense fluorescence: denying the presence of a heavy atom. *Angew. Chem., Int. Ed.* **2010**, *49*, 2349−2353. (e) Prusakova, V.; Mccusker, C. E.; Castellano, F. N. Ligand-localized triplet-state photophysics in a platinum(II) terpyridyl perylenediimideacetylide. *Inorg. Chem.* **2012**, *51*, 8589−8598. (f) Lentijo, S.; Aullón, G.; Miguel, J. A.; Espinet, P. Highly fluorescent complexes with gold, palladium or platinum linked to perylene through a tetrafluorophenyl group. *Dalton Trans.* **2013**, *42*, 6353−6365. (g) Nguyen, M. H.; Wong, C. Y.; Yip, J. H. K. Ligand perturbations on fluorescence of dinuclear platinum complexes of 5,12-diethynyltetracene: a spectroscopic and computational study. *Organometallics* **2013**, *32*, 1620−1629. (h) Steffen, A.; Costuas, K.; Boucekkine, A.; Thibault, M.; Beeby, A.; Batsanov, A. S.; Charafeddin, A.; Jacquemin, D.; Halet, J. F.; Marder, T. B. Fluorescence in rhoda- and iridacyclopentadienes neglecting the spin−orbit coupling of the heavy atom: the ligand dominates. *Inorg. Chem.* **2014**, *53*, 7055−7069. (i) Steffen, A.; Ward, R. M.; Tay, M. G.; Edkins, R. M.; Seeler, F.; Van, L. M.; Pålsson, L. O.; Beeby, A.; Batsanov, A. S.; Howard, J. A. Regiospecific formation and unusual optical properties of 2,5-bis(arylethynyl)rhodacyclopentadienes: a new class of luminescent organometallics. *Chem. - Eur. J.* **2014**, *20*, 3652−3666.

(4) (a) Petoud, S.; Muller, G.; Moore, E. G.; Xu, J.; Sokolnicki, J.; Riehl, J. P.; Le, U. N.; Cohen, S. M.; Raymond, K. N. Brilliant Sm, Eu, Tb, and Dy chiral lanthanide complexes with strong circularly polarized luminescence. *J. Am. Chem. Soc.* **2007**, *129*, 77−83. (b) D'Aléo, A.; Picot, A.; Beeby, A.; Williams, J. A. G.; Guennic, B. L.; Andraud, C.; Maury, O. Efficient sensitization of europium, ytterbium, and neodymium functionalized tris-dipicolinate lanthanide complexes through tunable charge-transfer excited states. *Inorg. Chem.*

DOI: 10.1021/acs.inorgchem.8b02376
Inorg. Chem. 2019, 58, 1806−1814

2008, *47*, 10258−10268. (c) Hardy, E. E.; Wyss, K. M.; Keller, R. J.; Gorden, J. D.; Gorden, A. Tunable ligand emission of napthylsalophen triple-decker dinuclear lanthanide(iii) sandwich complexes. *Dalton Trans.* **2018**, *47*, 1337−1346. (d) Bourdolle, A.; Allali, M.; Mulatier, J. C.; Le Guennic, B.; Zwier, J. M.; Baldeck, P. L.; Bünzli, J.-C. G.; Andraud, C.; Lamarque, L.; Maury, O. Modulating the photophysical properties of azamacrocyclic europium complexes with charge-transfer antenna chromophores. *Inorg. Chem.* **2011**, *50*, 4987−4899. (e) Butler, S. J.; Lamarque, L.; Pal, R.; Parker, D. EuroTracker dyes: highly emissive europium complexes as alternative organelle stains for live cell imaging. *Chem. Sci.* **2014**, *5*, 1750−1756. (f) Soulié, M.; Latzko, F.; Bourrier, E.; Placide, V.; Butler, S. J.; Pal, R.; Walton, J. W.; Baldeck, P. L.; Guennic, B. L.; Andraud, C.; Zwier, J. M.; Lamarque, L.; Parker, D.; Maury, O. Comparative analysis of conjugated alkynyl chromophore−triazacyclononane ligands for sensitized emission of europium and terbium. *Chem. - Eur. J.* **2014**, *20*, 8636−8646. (g) Butler, S. J.; Delbianco, M.; Lamarque, L.; McMahon, B. K.; Neil, E. R.; Pal, R.; Parker, D.; Waltona, J. W.; Zwier, J. M. EuroTracker® dyes: design, synthesis, structure and photophysical properties of very bright europium complexes and their use in bioassays and cellular optical imaging. *Dalton Trans.* **2015**, *44*, 4791−4803. (h) Levoye, A.; Zwier, J. M.; Jaracz-Ros, A.; Klipfel, L.; Cottet, M.; Maurel, D.; Bdioui, S.; Balabanian, K.; Prezeau, L.; Trinquet, E.; Durroux, T.; Bachelerie, F. A broad G protein-coupled receptor internalization assay that combines SNAP-Tag labeling, diffusion-enhanced resonance energy transfer, and a highly emissive terbium cyptate. *Front. Endocrinol.* **2015**, *6*, 167.

(5) (a) Weissman, S. I. Intramolecular energy transfer the fluorescence of complexes of europium. *J. Chem. Phys.* **1942**, *10*, 214−217. (b) Bünzli, J.-C. G. Lanthanide luminescence for biomedical analyses and imaging. *Chem. Rev.* **2010**, *110*, 2729−2755. (c) Eliseeva, S. V.; Bünzli, J.-C. G. Lanthanide luminescence for functional materials and bio-sciences. *Chem. Soc. Rev.* **2010**, *39*, 189−227. (d) Eliseeva, S. V.; Bünzli, J.-C. G. Lanthanide luminescence for functional materials and bio-sciences. *Chem. Soc. Rev.* **2010**, *39*, 189−227. (e) Bulach, V.; Sguerra, F.; Hosseini, M. W. Porphyrin lanthanide complexes for NIR emission. *Coord. Chem. Rev.* **2012**, *256*, 1468−1478. (f) D'Aléo, A.; Pointillart, F.; Ouahab, L.; Andraud, C.; Maury, O. Charge transfer excited states sensitization of lanthanide emitting from the visible to the near-infra-red. *Coord. Chem. Rev.* **2012**, *256*, 1604−1620.

(6) (a) Pfeiffer, P.; Breith, E.; Lübbe, E.; Tsumaki, T. Tricyclische orthokondensierte Nebenvalenzringe. *Liebigs Ann. Chem.* **1933**, *503*, 84−130. (b) Atwood, D. A.; Harvey, M. J. Group 13 compounds incorporating salen ligands. *Chem. Rev.* **2001**, *101*, 37−52. (c) Dalla Cort, A.; De Bernardin, P.; Forte, G.; Mihan, F. Y. Metal-salophen-based receptors for anions. *Chem. Soc. Rev.* **2010**, *39*, 3863−3874.

(7) (a) Yang, X.; Wang, S.; Wang, C.; Huang, S.; Jones, R. A., Construction and luminescence properties of 4f and d-4f clusters with salen-type Schiff base ligands. In *Recent Development In Clusters Of Rare Earths And Actinides: Chemistry And Materials*, Zheng, Z., Ed.; Springer: 2017; Vol. *173*, pp 155−187. (b) Yang, X.; Jones, R. A.; Huang, S. Luminescent 4f and d-4f polynuclear complexes and coordination polymers with flexible salen-type ligands. *Coord. Chem. Rev.* **2014**, *273-274*, 63−75.

(8) (a) Fei, B.; Yan, P.; Liu, T.; Yang, F.; Li, G. Synthesis and NIR luminescence of a series of salen type erbium complexes. *J. Lumin.* **2016**, *177*, 380−386. (b) Kaczmarek, M. T.; Zabiszak, M.; Nowak, M.; Jastrzab, R. Lanthanides: Schiff base complexes, applications in cancer diagnosis, therapy, and antibacterial activity. *Coord. Chem. Rev.* **2018**, *370*, 42−54. (c) Woodruff, D. N.; Winpenny, R. E.; Layfield, R. A. Lanthanide single-molecule magnets. *Chem. Rev.* **2013**, *113*, 5110−5148. (d) Xu, L.-J.; Xu, G.-T.; Chen, Z.-N. Recent advances in lanthanide luminescence with metal-organic chromophores as sensitizers. *Coord. Chem. Rev.* **2014**, *273−274*, 47−62. (e) Jia, J.-H.; Li, Q.-W.; Chen, Y.-C.; Liu, J.-L.; Tong, M.-L. Luminescent single-molecule magnets based on lanthanides: design strategies, recent advances and magneto-luminescent studies. *Coord. Chem. Rev.* **2019**, *378*, 365.

(9) Lo, W. K.; Wong, W. K.; Wong, W. Y.; Guo, J.; Yeung, K. T.; Cheng, Y. K.; Yang, X.; Jones, R. A. Heterobimetallic Zn(II)-Ln(III) phenylene-bridged Schiff base complexes, computational studies, and evidence for singlet energy transfer as the main pathway in the sensitization of near-infrared Nd3+ luminescence. *Inorg. Chem.* **2006**, *45*, 9315−9325.

(10) (a) Wong, W. K.; Zhu, X.; Wong, W. Y. Synthesis, structure, reactivity and photoluminescence of lanthanide(III) monoporphyrinate complexes. *Coord. Chem. Rev.* **2007**, *251*, 2386−2399. (b) Yang, Z.-S.; Ning, Y.; Yin, H.-Y.; Zhang, J.-L. Lutetium(III) porphyrinoids as effective triplet photosensitizers for photon upconversion based on triplet-triplet annihilation (TTA). *Inorg. Chem. Front.* **2018**, *5*, 2291−2299.

(11) (a) Ru, J.; Gao, F.; Wu, T.; Yao, M. X.; Li, Y. Z.; Zuo, J. L. Enantiopure heterobimetallic single-chain magnets from the chiral Ru(III) building block. *Dalton Trans.* **2014**, *43*, 933−936. (b) Ning, Y.; Ke, X. S.; Hu, J. Y.; Liu, Y. W.; Ma, F.; Sun, H. L.; Zhang, J. L. Bioinspired orientation of beta-substituents on porphyrin antenna ligands switches ytterbium(III) NIR emission with thermosensitivity. *Inorg. Chem.* **2017**, *56*, 1897−1905. (c) Yu, F.; Cao, Z. H.; Ge, J. Y.; Sun, Y. C.; Ouyang, Z. W.; Zuo, J. L.; Wang, Z.; Kurmoo, M. Magnetostructural relationship for mu2-phenoxido bridged ferric dimers. *Dalton Trans.* **2017**, *46*, 4317−4324.

(12) Tang, J.; Xie, D.; Yin, H. Y.; Jing, J.; Zhang, J.-L. Cationic sulfonium functionalization renders Znsalens with high fluorescence, good water solubility and tunable cell-permeability. *Org. Biomol. Chem.* **2016**, *14*, 3360−3368.

(13) Lacroix, P. G.; Bella, S. D.; Ledoux, I. Synthesis and second-order nonlinear optical properties of new copper(II), nickel(II), and zinc(II) Schiff-base complexes. toward a role of Inorganic chromophores for second harmonic generation. *Chem. Mater.* **1996**, *8*, 541−545.

(14) Camp, C.; Guidal, V.; Biswas, B.; Pecaut, J.; Dubois, L.; Mazzanti, M. Multielectron redox chemistry of lanthanide Schiff-base complexes. *Chem. Sci.* **2012**, *3*, 2433−2448.

(15) (a) Abe, Y.; Takagi, Y.; Nakamura, M.; Takeuchi, T.; Tanase, T.; Yokokawa, M.; Mukai, H.; Megumi, T.; Hachisuga, A.; Ohta, K. Structural, photophysical, and mesomorphic properties of luminescent platinum(II)-salen Schiff base complexes. *Inorg. Chim. Acta* **2012**, *392*, 254−260. (b) Borisov, S. M.; Saf, R.; Fischer, R.; Klimant, I. Synthesis and properties of new phosphorescent red light-excitable platinum(II) and palladium(II) complexes with Schiff bases for oxygen sensing and triplet-triplet annihilation-based upconversion. *Inorg. Chem.* **2013**, *52*, 1206−1216.

(16) (a) Kachura, T. F.; Sevhenk, A.; Solovev, K. N.; Tsvirko, M. P. Intramolecular transfer of electronic excitation-energy in porphyrin complexes of ytterbium. *Dokl. Akad. Nauk. Sssr.* **1974**, *217*, 1121−1124. (b) Wong, C.-P.; Venteicher, R. F.; Horrocks, W. D., Jr. Lanthanide porphyrin complexes - potential new class of nuclear magnetic-resonance dipolar probe. *J. Am. Chem. Soc.* **1974**, *96*, 7149−7150. (c) Gouterman, M.; Schumaker, C. D.; Srivastava, T. S.; Yonetani, T. Absorption and luminescence of yttrium and lanthanide octaethylporphin complexes. *Chem. Phys. Lett.* **1976**, *40*, 456−461. (d) Bulach, V.; Sguerra, F.; Hosseini, M. W. Porphyrin lanthanide complexes for NIR emission. *Coord. Chem. Rev.* **2012**, *256*, 1468−1478. (e) He, H. S. Near-infrared emitting lanthanide complexes of porphyrin and bodipy dyes. *Coord. Chem. Rev.* **2014**, *273-274*, 87−99. (f) Ke, X. S.; Ning, Y.; Tang, J.; Hu, J. Y.; Yin, H. Y.; Wang, G. X.; Yang, Z. S.; Jie, J.; Liu, K.; Meng, Z. S.; Zhang, Z.; Su, H.; Shu, C.; Zhang, J.-L. Gadolinium(III) porpholactones as efficient and robust singlet oxygen photosensitizers. *Chem. - Eur. J.* **2016**, *22*, 9676−9686.

(17) Xie, D.; Jing, J.; Cai, Y.-B.; Tang, J.; Chen, J.-J.; Zhang, J.-L. Construction of an orthogonal ZnSalen/Salophen library as a colour palette for one- and two-photon live cell imaging. *Chem. Sci.* **2014**, *5*, 2318−2327.

(18) Che, C. M.; Kwok, C. C.; Lai, S. W.; Rausch, A. F.; Finkenzeller, W. J.; Zhu, N.; Yersin, H. Photophysical properties and OLED applications of phosphorescent platinum(II) Schiff base complexes. *Chem. - Eur. J.* **2010**, *16*, 233−247.

DOI: 10.1021/acs.inorgchem.8b02376
Inorg. Chem. 2019, 58, 1806−1814

(19) Fonseca, J.; Martinez, J.; Cunha-Silva, L.; Magalhães, A. L.; Duarte, M. T.; Freire, C. Insights into electronic and structural properties of novel Pd(II) salen -type complexes. *Inorg. Chim. Acta* **2010**, *363*, 4096−4107.
(20) (a) Uh, H.; Petoud, S. Novel antennae for the sensitization of near infrared luminescent lanthanide cations. *C. R. Chim.* **2010**, *13*, 668−680. (b) Zhang, K.; Zhang, L.; Zhang, S.; Hu, Y.; Zheng, Y.; Huang, W. Construction of identical [2 + 2] Schiff-base macrocyclic ligands by Ln(III) and Zn(II) template ions including efficient Yb(III) near-infrared sensitizers. *Inorg. Chem.* **2015**, *54*, 5295−5300.
(21) (a) Xu, H. B.; Zhang, L. Y.; Xie, Z. L.; Ma, E.; Chen, Z. N. Heterododecanuclear Pt(6)Ln(6) (Ln = Nd, Yb) arrays of 4-ethynyl-2,2'-bipyridine with sensitized near-IR lanthanide luminescence by Pt −> Ln energy transfer. *Chem. Commun.* **2007**, 2744−2746. (b) Zhang, L. Y.; Zhang, H. X.; Ye, S.; Wen, H. M.; Chen, Z. N.; Osawa, M.; Uosaki, K.; Sasaki, Y. A butadiyne-linked diruthenium molecular wire self-assembled on a gold electrode surface. *Chem. Commun.* **2011**, *47*, 923−925. (c) Wen, H.-M.; Wang, J.-Y.; Li, B.; Zhang, L.-Y.; Chen, C.-N.; Chen, Z.-N. Phosphorescent square-planar platinum(II) complexes of 1,3-Bis(2-pyridylimino)isoindoline with a monodentate strong-field ligand. *Eur. J. Inorg. Chem.* **2013**, *2013*, 4789−4798.
(22) Tobita, S.; Arakawa, M.; Tanaka, I. Electronic relaxation processes of rare-earth chelates of benzoyltrifluoroacetone. *J. Phys. Chem.* **1984**, *88*, 2697−2702.
(23) (a) Hariharan, P. C.; Pople, J. A. The influence of polarization functions on molecular orbital hydrogenation energies. *Theor. Chim. Acta* **1973**, *28*, 213−222. (b) Francl, M. M.; Petro, W. J.; Hehre, W. J.; Binkley, J. S.; Gordon, M. S.; DeFree, D. J.; Pople, J. A. Self-consistent molecular orbital methods. XXIII. A polarization-type basis set for second-row elements. *J. Chem. Phys.* **1982**, *77*, 3654−3665.
(24) (a) Andrae, D.; Haeussermann, U.; Dolg, M.; Stoll, H.; Preuss, H. Energy-adjustedab initio pseudopotentials for the second and third row transition elements. *Theor. Chim. Acta* **1990**, *77*, 123−141. (b) Martin, J. M. L.; Sundermann, A. Correlation consistent valence basis sets for use with the Stuttgart−Dresden−Bonn relativistic effective core potentials: The atoms Ga−Kr and In−Xe. *J. Chem. Phys.* **2001**, *114*, 3408−3420.
(25) Hay, P. J.; Wadt, W. R. Ab initio effective core potentials for molecular calculations. Potentials for K to Au including the outermost core orbitals. *J. Chem. Phys.* **1985**, *82*, 299−310.
(26) (a) Dapprich, S.; Frenking, G. Investigation of donor-acceptor interactions: a charge decomposition analysis using fragment molecular orbitals. *J. Phys. Chem.* **1995**, *99*, 9352−9362. (b) Lu, T.; Chen, F. A multifunctional wavefunction analyzer. *J. Comput. Chem.* **2012**, *33*, 580−592. (c) Xiao, M.; Lu, T. Generalized charge decomposition analysis (GCDA) method. *J. Adv. Phys. Chem.* **2015**, *04*, 111−124.
(27) Snijders, J.; Baerends, E.; Ros, P. A perturbation theory approach to relativistic calculations: II. *Mol. Phys.* **1979**, *38*, 1909−1929.
(28) (a) Samanta, P. K.; Kim, D.; Coropceanu, V.; Bredas, J. L. Up-conversion intersystem crossing rates in organic emitters for thermally activated delayed fluorescence: impact of the nature of singlet vs triplet excited states. *J. Am. Chem. Soc.* **2017**, *139*, 4042−4051. (b) Ming Tong, G. S.; Chan, K. T.; Chang, X.; Che, C.-M. Theoretical studies on the photophysical properties of luminescent pincer gold(iii) arylacetylide complexes: the role of π-conjugation at the C-deprotonated [C^N^C] ligand. *Chem. Sci.* **2015**, *6*, 3026−3037. (c) Schmidt, K.; Brovelli, S.; Coropceanu, V.; Beljonne, D.; Cornil, J.; Bazzini, C.; Caronna, T.; Tubino, R.; Meinardi, F.; Shuai, Z.; Brédas, J.-L. Intersystem crossing processes in nonplanar aromatic heterocyclic molecules. *J. Phys. Chem. A* **2007**, *111*, 10490−10499.
(29) (a) Che, C. M.; Chan, S. C.; Xiang, H. F.; Chan, M. C.; Liu, Y.; Wang, Y. Tetradentate Schiff base platinum(II) complexes as new class of phosphorescent materials for high-efficiency and white-light electroluminescent devices. *Chem. Commun.* **2004**, 1484−1485. (b) Wu, P.; Ma, D.-L.; Leung, C.-H.; Yan, S.-C.; Zhu, N.; Abagyan, R.; Che, C.-M. Stabilization of G-Quadruplex DNA with platinum(II) Schiff base complexes: luminescent probe and down-regulation of c-myc oncogene expression. *Chem. - Eur. J.* **2009**, *15*, 13008−13021. (c) Tang, J.; Cai, Y.-B.; Jing, J.; Zhang, J.-L. Unravelling the correlation between metal induced aggregation and cellular uptake/subcellular localization of Znsalen: an overlooked rule for design of luminescent metal probes. *Chem. Sci.* **2015**, *6*, 2389−2397. (d) Tang, J.; Zhang, M.; Yin, H. Y.; Jing, J.; Xie, D.; Xu, P.; Zhang, J.-L. A photoactivatable Znsalen complex for super-resolution imaging of mitochondria in living cells. *Chem. Commun.* **2016**, *52*, 11583−11586. (e) Tang, J.; Zhang, Y.; Yin, H. Y.; Xu, G.; Zhang, J.-L. Precise labeling and tracking of lipid droplets in adipocytes using a luminescent ZnSalen complex. *Chem. - Asian J.* **2017**, *12*, 2533−2538. (f) Tzubery, A.; Melamedbook, N.; Tshuva, E. Y. Fluorescent antitumor titanium(iv) salen complexes for cell imaging. *Dalton Trans.* **2018**, *47*, 3669−3673.
(30) (a) Consiglio, G.; Failla, S.; Finocchiaro, P.; Oliveri, I. P.; Di Bella, S. Aggregation properties of bis(salicylaldiminato)zinc(II) Schiff-base complexes and their Lewis acidic character. *Dalton Trans.* **2012**, *41*, 387−395. (b) Consiglio, G.; Failla, S.; Oliveri, I. P.; Purrello, R.; Di Bella, S. Controlling the molecular aggregation. An amphiphilic Schiff-base zinc(II) complex as supramolecular fluorescent probe. *Dalton Trans.* **2009**, 10426−10428. (c) Consiglio, G.; Failla, S.; Finocchiaro, P.; Oliveri, I. P.; Di Bella, S. An unprecedented structural interconversion in solution of aggregate zinc(II) salen Schiff-base complexes. *Inorg. Chem.* **2012**, *51*, 8409−8418.

DOI: 10.1021/acs.inorgchem.8b02376
Inorg. Chem. 2019, 58, 1806−1814